**Photoactivity under visible light of defective ZnO investigated by EPR spectroscopy and photoluminescence**

# Photoactivity under visible light of ZnO prepared by wet chemistry

Erik Cerrato, Maria Cristina Paganini*, Elio Giamello

Dipartimento di Chimica, Via giuria 7, 10126, Torino

*Corresponding author email: mariacristina.paganini@unito.it*

**Abstract**: The photochemical and the photophysical properties of a defective zinc oxide prepared by precipitation have been investigated using mainly Electron Paramagnetic Resonance (EPR) and Photoluminescence (PL) spectroscopy. As already reported in the literature the band gap of the oxide contains intra band gap states related to the presence of point defects (mainly cation vacancies) in the structure. The concentration and the energy levels of such a defect are the basis of mechanisms of double and multiple excitations allowing low energy visible photons ($h\nu < E_g$) to promote electrons from the valence band to the conduction band similarly, though low efficiently, to what done by UV light with $h\nu > E_g$. Since a robust fraction of the visible light generated carriers reach the surface of the nanocrystals, where they entail the typical redox reactions of photocatalysis including formation of hydroxyl radicals the wet chemistry prepared zinc oxide can be considered a Visible Light Active (VLA) system.

**Keywords:** ZnO defects, photoactivity, visible light irradiation

## 1. Introduction

In recent years the scientific community is paying an increasing attention to the area of photocatalysis. Photocatalytic processes aim to exploit light energy to promote chemical transformations. This scope can be pursued in various applications including pollution remediation (total oxidation of pollutants [1-3]), solar fuel production (e.g. water photosplitting and $CO_2$ reduction [4]) and, more generally, in all types of chemical processes in which the required thermal energy can be replaced by electromagnetic energy.

A standard photocatalytic process is based on the photoexcitation of a suitable semiconducting system inducing the promotion of electrons in the conduction band (CB) and the formation of electron-holes (holes, $h^+$) in the valence band (VB). The reductive and oxidative capacities of these photo-excited charge carriers (essential to the redox processes at the base of the photocatalytic action) depend on the chemical potentials of CB and VB, respectively.

The materials that have so far dominated the field of environmental photocatalysis are based on titanium dioxide or other semiconductors with high band gap, whose excitation requires the use of UV radiation. Actually many processes in this field are already implemented on a small and medium scale using ultraviolet artificial radiation. However, it is clear that an upgrade of these processes to large-scale plants requires a transition to the use of sunlight that means, on the basis of the solar spectrum at the earth's surface, essentially visible frequencies.

During the first two decades of this century an intense effort has been devoted to the search for innovative photocatalytic systems capable of working under visible light illumination. The approaches followed to this aim include the use of: i) small band gap semiconductors such as, for instance, the recently applied $C_3N_4$ systems [5-7] (in this case it is impossible to have simultaneously favourable both reduction and oxidation potentials); ii) semiconducting systems with band gap modified by the insertion of impurities (like in the case of the well-known N doped $TiO_2$) [8-10]; iii) coupled semiconductors reproducing either the so-called Z scheme [4, 11] of natural photosynthesis or the recently proposed S-scheme [6, 12]. In both cases, distinct photocatalysts carry out reduction and oxidation, respectively. In this case a molecular redox shuttle is usually employed to connect the two systems through the liquid phase.

Systems in some way related to this latter model are those based on two different solids put in contact through a solid-solid interface, called heterojunction, that often exhibit peculiar electronic properties different from those of the individual components. A case recently tackled in our laboratory is that of the $CeO_2$-ZnO system in which particles of cerium dioxide are deposited on the

surface of the majority component, the semiconducting zinc oxide. This novel system has revealed an excellent ability to work as a photocatalyst in the abatement of emerging pollutants using visible light [13-17]. A detailed investigation of the photocatalyst has put into evidence the presence of states at the interface between $CeO_2$ and ZnO that allow the excitation, promoted by photons of the visible range, of electrons from the valence band of zinc oxide to 4f states of cerium dioxide. This excitation represents the initial step of the photocatalytic process driven by visible light [18, 19]. However, during the investigation of $CeO_2$-ZnO it became evident that the zinc oxide matrix present in the $CeO_2$-ZnO mixed system is itself influenced by visible irradiation. This observation prompted us to deal with a specific study on the photophysics and photochemistry of pristine ZnO (prepared in a way analogous to that adopted for $CeO_2$-ZnO) that is reported in the present paper. The subject is indeed not new, however a scrutiny of the literature in the field indicates that the majority of studies have been devoted to single crystals of high purity prepared for microelectronic and optoelectronics applications [20-26] while some others are performed on materials that underwent deep modifications by high energy irradiation with neutron or high energy electron beams in order to describe the defects generated in the crystalline structure by the heavy treatments.

In the present study we have employed various techniques to characterize nanostructured zinc oxide prepared by wet chemistry methods and calcined after drying, with a particular emphasis on the results obtained by Electron Paramagnetic Resonance (EPR). This technique is less known to the research community working on the optoelectronic properties of solid materials, if compared with other techniques like Photoluminescence (PL). EPR however has high importance both in the investigation of defects in the solid state and in those related to photocatalysis. In the former case EPR permits to unravel the features (nature, symmetry, electron spin density distribution) of paramagnetic point defects. These represent an important fraction of the whole defectivity in ionic and covalent solids and, due to the high sensitivity of EPR, very small concentrations of defects can be detected. In the area of photochemistry and photocatalysis the importance of EPR is related to the phenomena of photo-induced charge separation and, in particular, to the stabilisation or reaction of the charge carriers so generated. Addition of an electron and/or of a hole to a usually diamagnetic entity produce in fact paramagnetic centres that are conveniently investigated by EPR [8, 27-31]

We will show, in the following, that polycrystalline zinc oxide materials prepared by wet chemistry methods have a rich and complex defect structure that deeply influences the band gap of the solid

and brings about amazing photophysical properties when irradiated with visible frequencies. Quite similar results have been obtained investigating samples prepared by precipitation from a solution with those synthetized by hydrothermal methods. For the sake of simplicity, we will report the results obtained on the former material only, comparing them with what observed in the case of a well-known commercial material prepared by ignition of metallic zinc which is highly crystalline and much less defective than the wet-chemistry prepared oxides. The results of the present investigation are of interest on the one hand because of the inherent importance of ZnO in heterogeneous photocatalysis and, on the other hand, to better understand the features and the behaviour of more complex photocatalysts such as the recently reported $CeO_2$-ZnO mixed system.

## 2. Materials and Methods

### 2.1 Samples preparation

For the production of bare ZnO a precipitation synthesis route was employed, starting from zinc acetate dihydrate, received by Sigma Aldrich and used without any further purification treatment [32]. This preparation method guaranties low-cost production of ZnO with the advantage of being environmental-friendly, since it prevents the use of surfactants and organic solvents. ZnO was synthetized dissolving 2.2 g of $Zn(CH_3COO)_2 \cdot 2H_2O$ into 160 mL of distilled water and 80 mL of ethanol and left in stirring for 1 h. Subsequently, 160 mL of NaOH 1M was added at room temperature, leading to form a white precipitate that was separated via filtration ad washed with water and ethanol. The precipitate was dried at 70°C for 12 h and finally calcined for 30 h at 300°C. We will indicate this material in the following simply as ZnO. Kadox ZnO was purchased from Sigma-Aldrich. This material is prepared by direct ignition of metallic zinc and is highly crystalline. It was used in this work as a reference to compare with the material synthetized by precipitation.

The samples used in in the experiments reported in Section 3.3 and 3.4 were submitted to an activation treatment in the aim both of cleaning the surface from hydroxyl and carboxyl groups, obtaining a material as close as possible to the stoichiometric ratio. The treatment involves an annealing at 573 K in dynamic vacuum ($10^{-4}$ mbar) for 30 minutes, followed by the re-oxidation at 673 K in oxygen atmosphere (50 mbar) for 1 h. Finally, the molecular oxygen was removed from the cell at room temperature before the measurements were carried on.

### 2.2 Samples Characterization

The structural and morphological features of the synthetized sample were studied employing X-rays diffraction (XRD), Transmission Electron microscopy (TEM) and $N_2$ adsorption for area measure (BET).

X-rays diffraction patterns were recorded with a PANalytical PW3040/60 X'Pert PRP MPD using a cupper Kα radiation source of 0.154056nm. The reflections were scanned continuously in the 2θ ranges from 20° to 80°. Phase identification was performed using the X'Pert High-Score software. Scherrer equation was applied to evaluate the crystallite size of the existing phases.

A Micromeritics ASAP 2020 for $N_2$ adsorption measurement was employed in order to evaluate the sample specific surface areas. Prior to the absorption run, all the samples were outgassed at 573K for 2 hours.

The high resolution TEM images were achieved with a JEOL JEM 3010UHR (300 kV) apparatus; samples were dry deposited on Cu "holey" carbon grids.

The UV-vis absorption spectra were recorded using a Varian Cary 5 spectrometer, equipped with an integration sphere for diffuse reflectance (DR) studies, using a Carywin-UV / scan software. A Teflon sample with 100% reflectance was used as reference.

The optical band gap energies were calculated considering that the energy dependence of the absorption coefficient (α) for semiconductors in the region near the absorption edge is given by:

$$\alpha \propto \frac{(h\nu - E_{bg})^{\eta}}{h\nu}$$

Where hν is the energy of the incident photon and $E_{bg}$ is the optical absorption energy. η depends on the type of optical transition and since ZnO shows a direct-allowed optical transition its value is 1/2. Finally, since the scattering coefficient weakly depends on energy and $F(R_\infty)$, it can be assumed as proportional to the absorption coefficient within the narrow range of energy containing the absorption edge feature.

$$F(R_\infty) = \frac{(h\nu - E_{bg})^{\eta}}{h\nu}$$

Then, the plot $(F(R_\infty)*h\nu)^{1/\eta}$ vs hν can be used to determine the absorption edge energy (Tauc plot) method.

Electron Paramagnetic Resonance spectra were recorded using an X-band CW-EPR Bruker EMX spectrometer equipped with a cylindrical cavity operating at 100 KHz field modulation. The measurements were recorded at liquid nitrogen temperature (77K). The photochemistry of the material was investigated by situ irradiation in the EPR cavity, using a 1000W xenon lamp (Oriel

Instruments) equipped with an IR water filter, which provides a continuous photon flux from 250 to 750nm. During the experiments, different band-pass filters were employed (Newport-20CGA) at 400nm, 420nm, 455nm and 495nm: these kind of filters provide a good coverage with a range of ±10 nm. The irradiance for the different band-pass filters were considered in order to normalize the contribution of each filter using an experimental set up reproducing the conditions of the irradiation into the EPR cavity, similar to that used for illumination in the EPR cavity. The irradiance was measured at 50 cm from the source with a Delta OHM HD 2302.0 LightMeter. The values reported in Fig. 4B, 5B and 6B (irradiation experiments) are normalized on the irradiance values measured in this way. Specific experiments of irradiation under monochromatic light were performed by means of LED lamps emitting at 465±20 nm, 522±20 nm and 634±20 nm (Blue, green and red), respectively. The relative emission spectra are reported in the Supporting Information (fig S4).

The migration of the photo-generated charge carriers through the solid was evaluated performing irradiations in 20 mbar oxygen and hydrogen atmosphere, respectively.

The formation of $OH^{\bullet}$ radical species upon irradiation was monitored by the EPR spin trapping technique using a Miniscope 100 spectrometer from Magnetech and using DMPO as spin trapping agent.

Photoluminescence spectra were recorded on a FLS980 PL spectrometer from Edinburgh Instruments with a polychromatic 450 W Xe-arc lamp. A front-facing sample holder suitable for powder samples constituted the measurement assembling and the spectra were registered at room temperature.

## 3 Experimental results

### 3.1 Structural analysis and optical investigations

The ZnO material synthetized by precipitation shows the typical XRD pattern of the ZnO wurtzitic hexagonal phase (00-036-1451 ICDD pattern) [33]. The reported pattern indicates the absence of impurity phases in the synthetized sample. In addition, the sharp reflection peaks indicate the good crystallinity of the material. In order to evaluate the average crystal size, the Scherrer equation was applied on the first five reflections of the XRD pattern obtaining an average crystalline size of 338±21 nm which becomes about 500 nm in the case of Kadox. The latter sample shows, as expected, an even higher crystallinity than ZnO. (Fig. S1 in Supporting Information)

TEM images of ZnO, reported in Figure 1, partially confirm the above results. Indeed, it is possible to observe very large particles with size similar to that predicted from Scherrer analysis, but also

particles of very much lower sizes, mostly around 30 nm, that decorate the larger ones. Finally, it emerges that both larger and small particles exhibit platelet shape.

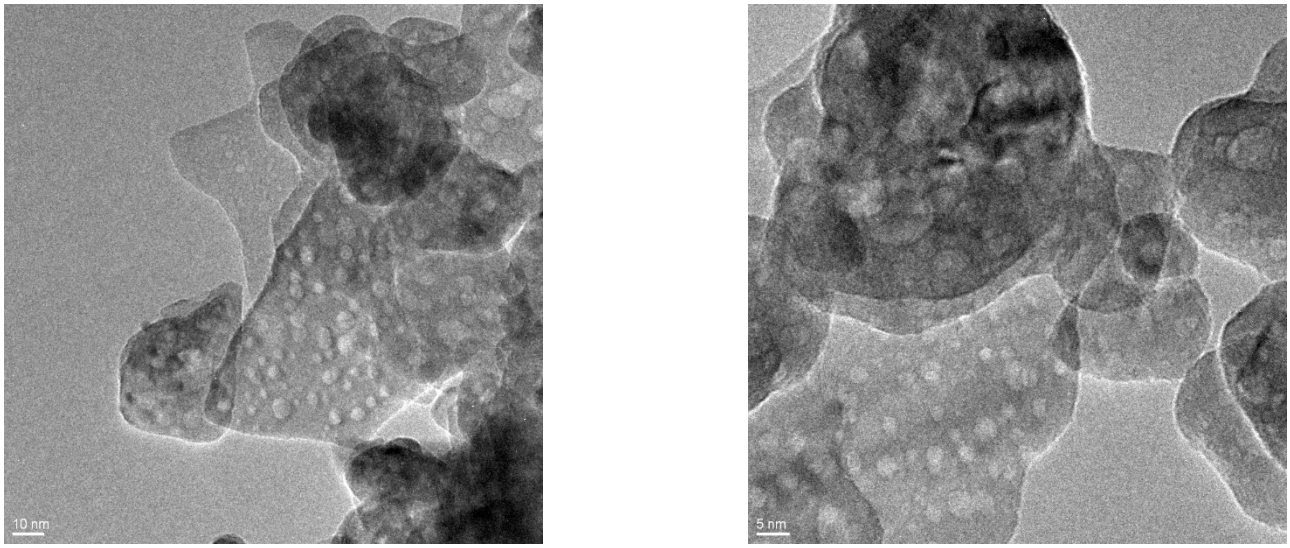


**Figure 1.** TEM images of ZnO crystals.

The specific surface area, evaluated with the BET method, revealed a value of 21 $m^2/g$ for ZnO in line with the well-known difficulty of obtaining high surface area ZnO materials. The specific surface area of Kadox ZnO is less than 10 $m^2/g$ [34].

DR-UV-Vis spectra of the as prepared material both in absorbance and reflectance units (Figure 2) show the typical valence band – conduction band transition of ZnO [35].

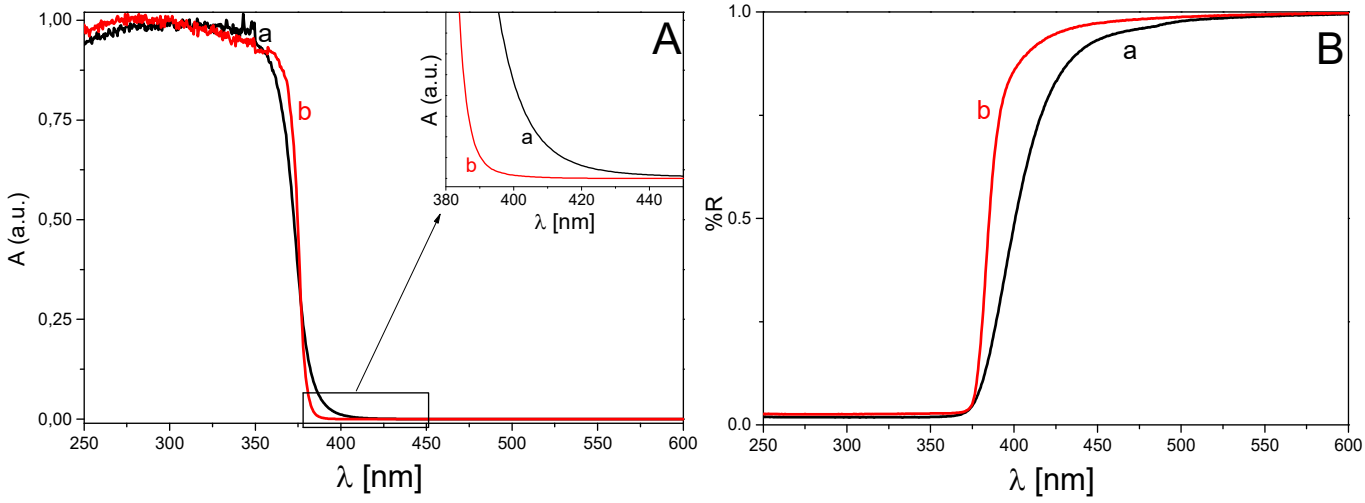


**Figure 2.** Panel A: DR-UV-Vis spectra (Kubelka-Munk transformed) of ZnO (a) and ZnO Kadox (b). Panel B: Normalized Diffused Reflectance spectra.

However, in the case of ZnO, this transition is less sharp than in the case of Kadox and some optical absorption between 380 nm and 440 nm seems to be present, as confirmed by the zoom in Fig. 2A.

The energy gap of ZnO , evaluated by means of the Tauc equation [36], gives a value of 3.28 eV, in line with the value of 3.3 eV reported in literature [37].

### 3.2 EPR spectroscopy upon irradiation under vacuum

The EPR spectrum of the as prepared ZnO material (Fig. 3a) recorded in dark is not a flat line. It shows in fact the presence of signals both at $g>g_e$ (left hand side of the spectrum) and at $g<g_e$ (right hand side, while $g_e$ = 2.0023 is the free electron g value). This indicates that some (paramagnetic) defects are already present in the as prepared materials. Both the global intensity and the ratio between the intensities of the two main signals in Fig. 3a (symmetric lines at g= 1.96 and g= 2.014) and always present in freshly prepared solids have a slightly variable value for different samples. We will show in the following that the majority of these defects derives from the exposure of the materials to the ambient light after preparation. The background observed for Kadox ZnO is similar to that in Fig. 3a but far less intense, confirming the lower defectivity of this highly crystalline material (Fig. S2).

When a semiconductor oxide is irradiated with photons whose energy is larger than the material band gap, an electron is promoted from the valence band to the conduction band with the formation of an electron hole (or simply hole) in the valence band; the phenomenon is described in the following equation:

$$MeO_X + h\nu \rightarrow e^-_{(CB)} + h^+_{(VB)} \qquad (2)$$

At this stage, the photo-generated charge carriers can recombine (with loss of the photon energy) or migrate through the solid. If the irradiation is performed in vacuum condition, in the absence of possible reactive molecules at the interface between the solid and the external fluid phase, the stabilization of a fraction of the photogenerated charge carriers can be observed by EPR either under irradiation or after irradiation provided that the temperature is kept low enough to prevent recombination. In a semiconducting oxide electron holes are stabilized by oxygen ions while excited electrons are usually associated to some cation sites [40, 41]. Fig. 3b shows the effect of irradiation with polychromatic UV light only ($\lambda$ < 370 nm, E>3.35 eV) on a sample of ZnO. The frequencies employed are such to allow the excitation of electrons from the valence band to the conduction band. The irradiation causes the growth of all the signals already present in the background except the symmetric line at g = 2.014 that is not affected by UV-irradiation. The relatively complex signal in the region of $g > g_e$ (the g values derived from simulation are listed in Table 1) is analogous to

those observed in the case of various irradiated oxides and is due to the trapping of photo-generated holes taking place according to equation 3:

$$h^{+}_{(VB)} + O^{2-} \rightarrow O^{-} \qquad (3)$$

The g values of this signal are totally compatible with the expected values for a $O^{-}$ center [28, 38-40] that is an electron hole trapped onto an oxygen $O^{2-}$ ion.

The trapping of photo-generated electrons is responsible of the symmetric signal centered at g = 1.96 (right hand side of the Figure). In various cases [40, 41] the photogenerated electron is directly stabilized on a specific cation (*e.g.* $Ti^{4+}$ in $TiO_2$) while in this case the signal at g = 1.96 is more likely associated to electrons in the conduction band or in a band built up by donor levels just below the bottom of the conduction band [41, 42]. The mechanism reported in equation 4:

$$e^{-} + Zn^{2+} \rightarrow Zn^{+} \qquad (4)$$

is therefore purely formal and can be accepted taking into account that the conduction band in ZnO is based on empty 4s and 4p Zn orbitals. We have thus identified the traces related to the stabilization of electron and holes when a VB to CB excitation is performed. The state corresponding to the signal at g = 2.014 must be related to some intra band gap state (see below). With this simple result in mind we can now analyze the somehow amazing results related to the irradiation of ZnO using visible frequencies.

| Nature of the species | | g tensor |
|---|---|---|
| trapped electrons | $Zn^{+}$ | g = 1.96 (isotropic) |
| trapped holes | $O^{-}$ | $g_{\perp}$ = 2.021, $g_{//}$ = 2.003 (axial) |
| trapped holes | $O^{-}$ | $g_{\perp}$ = 2.009, $g_{//}$ = 2.004 (axial) |
| Background signal | / | g = 2.014 (isotropic) |

*Table 1. Origins and g values of the observed EPR signals in ZnO spectra.*

Fig. 3 (c-f) reports the EPR spectra at 77 K obtained irradiating ZnO with polychromatic visible light. Irradiation was performed using band-pass filters at progressively increasing wavelength. In particular, all the selected radiations are beyond the UV-vis limit (380 nm) and, in any case, have energy always lower than the band gap value (3.28 eV) measured for ZnO (Fig. 2). In all cases we observe the same phenomena described in Fig. 3b i.e. the stabilization of photogenerated electrons

(signal at g = 1.96) and holes (g > 2.0023). This means that visible frequencies are able to induce phenomena of charge separation in the polycrystalline ZnO material here investigated analogous to that illustrated in Fig. 3b, observed under UV irradiation. The only qualitative difference concerns the symmetric signal at g = 2.014 present in the background that totally or partially vanishes in all cases of visible illumination while it is unaffected under UV.

The phenomenon of charge separation occurs at different extent according to the selected filter as illustrated Fig. 4 where each pair of histograms corresponds to the integrated intensity (hence to the amount of paramagnetic centers) of the two main EPR signals (trapped holes and trapped electrons respectively. The intensity reported in Fig. 4 are apparently conflicting with those perceived by Fig 3. Actually, it must be taken into account that in each of the reported experiments the photon flux is different because of the different cut-off performed in each case. Fig. 4 have been built up normalizing the intensity of the irradiance of the lamp in each experiments and subtracting the background (Fig. 3a) intensity.

The results for Kadox shows a lower increase of the EPR signals upon irradiation with respect to ZnO (Fig. S2 and S3), imputable to the higher crystallinity of the material and to the corresponding lower concentration of lattice defects.

The charge separation ability exerted by visible light evaluated in quantitative terms is not a minor feature and, though the lower true flux of UV-light, is comparable with that monitored in several other cases with the same EPR approach [27, 29, 43-46].

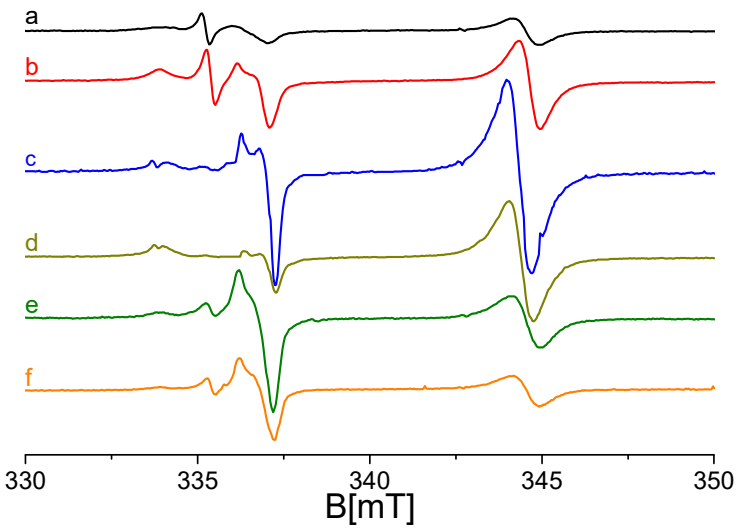


**Figure 3.** *(a) EPR spectra at 77K of activated ZnO, (b) after irradiation with UV light, λ<370 nm, (c) λ>400 nm, (d) λ>420nm, (e) λ>455nm and (f) λ>495nm.*

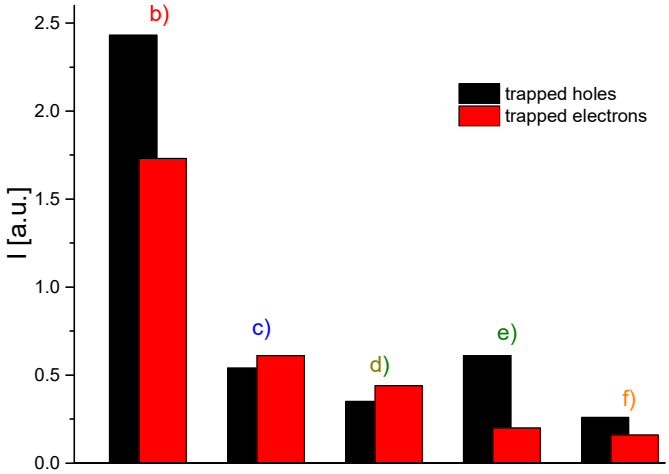


**Figure 4.** *Intensity of doubly integrated EPR signals (trapped holes and trapped electrons) as a function of the irradiated wavelength and normalized on irradiances. The intensity of the starting signals of spectrum 3a of Fig3 (background) has been subtracted from the experimental values.*

The quantitative aspect of the experiments in Fig. 3 and 4 (that are, by the way, fully reproducible) can be resumed as follows: i) the effect of charge separation seems to decline moving the cut-off from values close to the band gap transition towards higher wavelength (with the only exception of case 4d) ($\lambda$>455 nm) ii) in all cases the amount of trapped electron and trapped holes is similar except, again, the case 4d) with an amount of trapped holes which is about three times that of trapped electrons.

After each experiment of irradiation, the solids were warmed till room temperature in order to monitor charge recombination. The EPR spectra recorded after cooling again the solid indicate that recombination has occurred at a large extent but not completely since the starting situation (Fig. 3b) is never fully recovered.

The peculiar behavior of polycrystalline zinc oxide, upon visible irradiations, is not totally unknown to the literature but the mechanism behind visible photon absorption is still incompletely explained [19, 47-52]. The basic, though coarse, information derived from the experiments under visible light is that the photogeneration and stabilization of electrons and holes can be attained using a photon energy definitely lower than the band gap value (3.28 eV) with a result analogous to that illustrated in Fig. 3b, obtained by UV irradiation. This finding can only be explained admitting both the presence of a rich set of intra band gap defects and the existence of a complex interplay during irradiation involving the electrons of the valence band and those of the intra-band gap states. The results of the experiments in Fig. 3-4 cannot allow a detailed description of the energy states present in the band gap since they have been obtained using multi-frequency light beams. Polychromatic

irradiation is however important, to the aim of our work, since it is same type of illumination employed in experiments of photocatalysis and it has allowed to recognize that the solid here considered is sensitive to visible light.

The described behavior of the system supports the idea of the existence of a complex distribution of states in the band gap playing a role in the photochemistry of the material upon visible light absorption. This aspect will be further investigated by Photoluminescence spectroscopy (see below).

In order to shade some light on the blurred picture derived from polychromatic irradiation we have also recorded EPR spectra upon quasi-monochromatic irradiation obtained using a set of three LED lamps emitting with a maximum of 465 nm (blue), 522 nm (green) and 634 nm (orange-red) respectively (see S.I. for the plot of emission the lamps, Fig. S4).

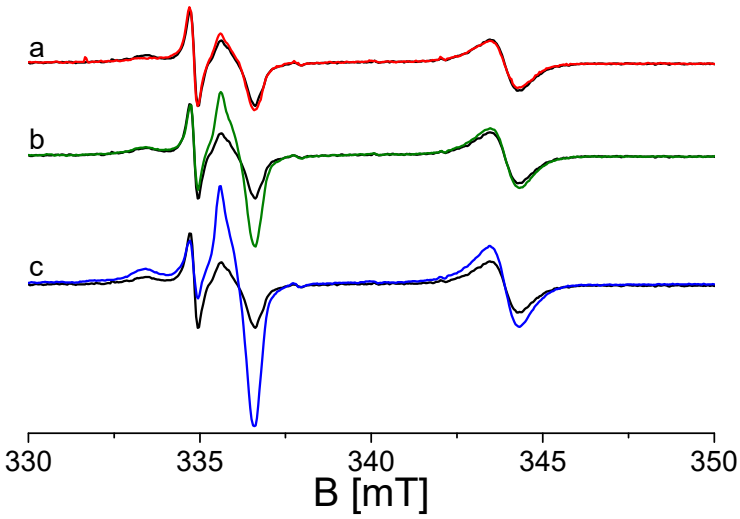


**Figure 5.** *EPR spectra of synthetized ZnO irradiated with: a) monochromatic red light (red line), b) monochromatic green light (green line) and c) monochromatic blue light (blue line). The spectrum before the irradiation is reported for comparison (black line).*

In figure 5 the result of each irradiation is compared with the background (spectrum recorded in the dark). Due to the different irradiance of the two light emitting systems (polychromatic and monochromatic light) the spectra in Fig. 5 have lower intensity than those in Fig. 3. The red light (5a) has no effect while illumination with both green (5b) and blue (5c) light causes an effect of charge separation which is more pronounced in the second case. In both these cases however the amount of trapped holes (l.h.d of the spectrum) observed exceed that of trapped electrons (r.h.s., signal at g = 1.96) thus suggesting, like in the case of Fig. 3-4 e), that a fraction of the excited electrons is not detectable.

**3.3 EPR spectroscopy upon irradiation under reactive atmosphere and in water.**

In order to evaluate the migration of photo-generated charge carriers through the solid, we performed irradiations both in oxygen and hydrogen atmosphere using full lamp irradiation (UV-Vis) and, in a second case, a band-pass filter at 400 nm (Vis). These two gases are expected to react with electrons and holes respectively provided that an appreciable fraction of the photogenerated charge carrier reach the surface of the solid.

It is well-established that $O_2$ can act as an electron scavenger at the surface forming the paramagnetic $O_2^-$ superoxide anion, that adsorbs on specific cationic sites

$$e^- + O_2(gas) \rightarrow O_2^-(ads)$$

In Fig. 6b the effect of UV irradiation is reported that leads, as expected, to the formation of the well-known signal of superoxide ions adsorbed on $Zn^{2+}$ cations with $g_{zz}$=2.050-2.055, $g_{yy}$=2.009 and $g_{xx}$=2.003 [53, 54]. Remarkably, irradiation with visible polychromatic light (Fig. 6c) also produces, though at minor extent, the typical profile of the superoxide ion which is detected for the components at g=2.009 and 2.003 (partially overlapped with the $O^-$ signal) while the $g_{zz}$ component (the weaker one) is in this case undetectable. The spectrum in Fig. 6c is however sufficient to indicate that a few electrons excited by a mix of visible frequencies can reach the surface where they reduce the oxygen molecule. A quantitative comparison of the results of photoexcitation under vacuum (Fig. 4) and in oxygen (Fig. 6) indicates however that it is indeed a minor fraction of the photogenerated electrons that has the ability to reach the surface of the solid becoming potentially available for reduction reactions. The growth of the signal at g = 1.96 (compare Fig. 6a and 6c) testifies that the main phenomenon in the case of visible polychromatic irradiation remains the charge separation described in the previous section.

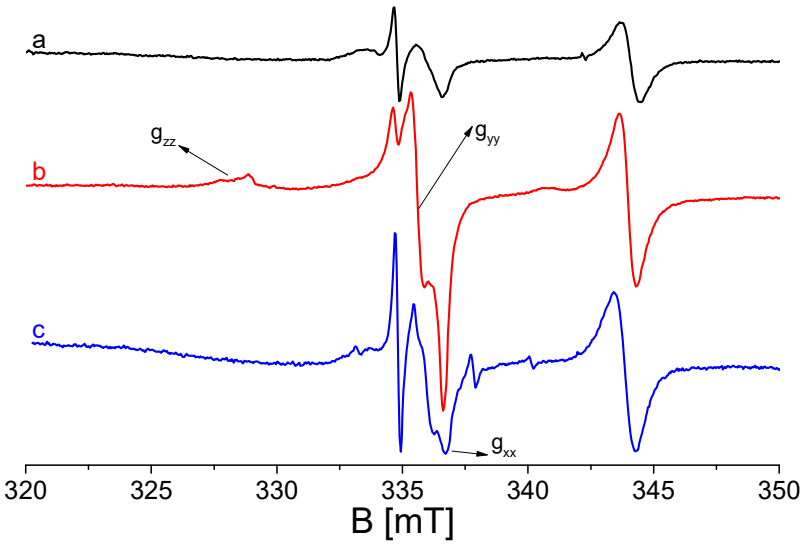


***Figure 6.*** *EPR spectra of: a) synthetized ZnO before irradiation (black line); b) irradiation with band-pass filter at λ≥400 nm in the presence of molecular oxygen.*

More effective is the reactivity at the surface of photogenerated holes. This has been monitored irradiating ZnO in $H_2$ atmosphere with UV (Fig. 7 panel A) and visible light (Fig 7 panel B). Hydrogen acts as a scavenger for the surface holes undergoing homolytic splitting and producing atomic hydrogen:

$$O^-_{(surf)} + H_{2\,(gas)} \rightarrow OH^-_{(surf)} + H^\bullet \qquad (7)$$

$H^\bullet$ is a powerful reducing agent [27, 55] able to inject electrons in the solid as monitored by the growth of the EPR signal at g = 1.96 indicating the formal (see before) reduction of $Zn^{2+}$

$$Zn^{2+} + O^{2-}_{(surf)} + H^\bullet \rightarrow OH^-_{(surf)} + Zn^+ \qquad (8)$$

In both panels of Fig. 7 we find that the spectrum b is uniquely due to trapped electrons (g = 1.96) and no trace of trapped hole is present. This means that all the holes generated by irradiation (UV or Vis) have reacted with hydrogen at the surface of the solid according to eqs. 7 and 8. Furthermore, the relatively high intensity of the spectrum in Fig. 7B(b) (visible light) surprisingly suggest that a significant production of reactive holes is induced, in zinc oxide produced by wet chemistry, by visible frequencies. This result cast new light on the photochemistry of this material.

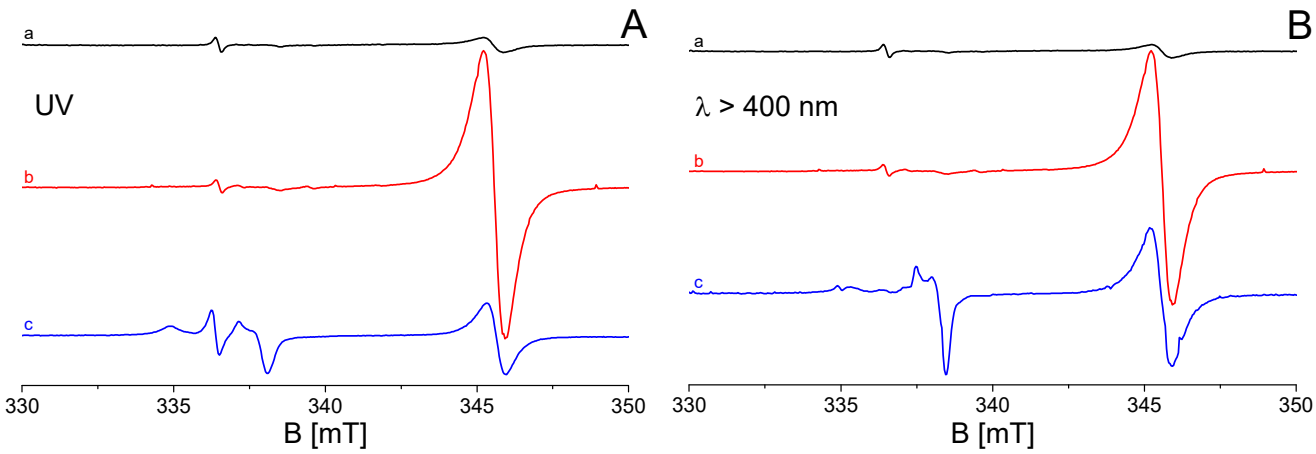


***Figure 7.*** *Panel A: ZnO EPR spectra at 77K: (a) background (dark), (b) after irradiation with UV light (λ<370nm) in the presence of $H_2$ and (c) after irradiation with UV light in vacuum. Panel B: ZnO EPR spectra at 77K: (a) background (dark), (b) after irradiation with visible light, λ≥400 nm in the presence of $H_2$, and (c) irradiation with visible light in vacuum.*

This finding is supported by the results of spin trapping in solution. The photoactivity at the solid-liquid interface has been assessed irradiating an aqueous suspension of the solid in presence of DMPO (5,5-dymethil-1-pyrroline-N-oxide), that acts as a spin trap of hydroxyl radicals ($OH^\bullet$) in solution forming a stable radical adduct (DMPO/ $OH^\bullet$) easily monitored by EPR spectroscopy [56]. The production of $OH^\bullet$ radicals under illumination, of crucial importance in photo-degradation processes, is ascribable to the reaction of water molecules or surface hydroxyl groups with photogenerated holes

$$h^+_{(VB)} + H_2O \rightarrow OH^\bullet + H^+ \qquad (6)$$

Fig. 8, panel A, reports the typical four line EPR spectrum of the DMPO-OH adduct formed upon UV and visible irradiation of ZnO as observed at a time corresponding to the maximum $OH^\bullet$ production in the two irradiation conditions. Board B reports the spin adduct concentration as a function of time. It shows that the maximum concentration is reached after 5 min in the case of UV light and after 30 min for visible irradiation. The maximum amount of photo-formed $OH^\bullet$ radicals is more than three times higher in the case of UV irradiation. However, the non-negligible photo-formation of $OH^\bullet$ under visible light is particularly significant since it is obtained with photons having energy smaller than the band gap value.

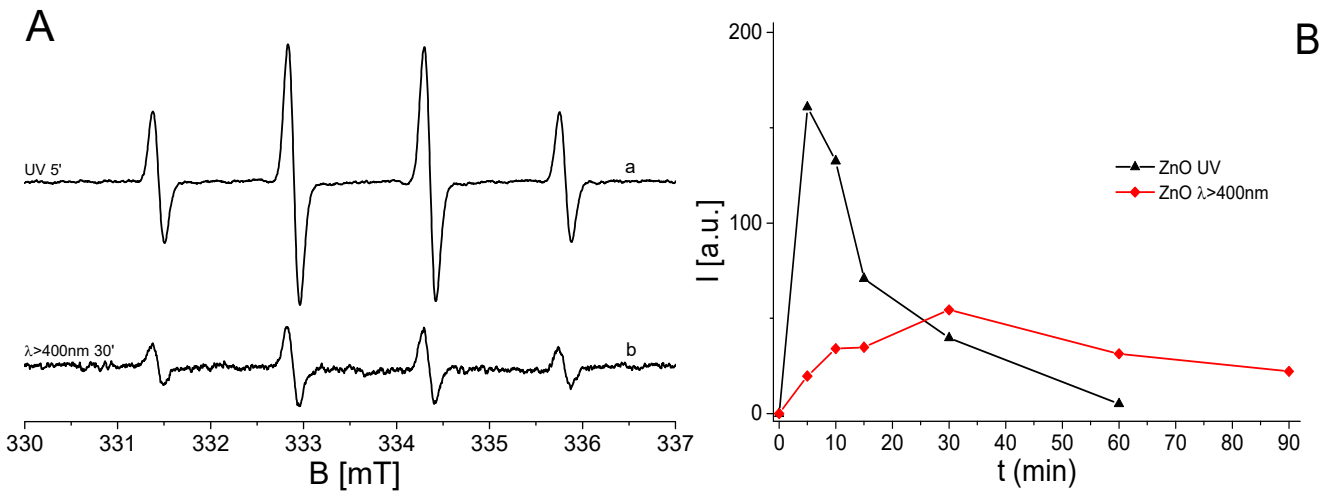


***Figure 8.*** *Panel A: EPR spectra of the DMPO/OH• adduct produced by irradiation of an aqueous suspensions of ZnO with UV (a) and visible (λ≥400 nm) light (b) at the maximum of OH• production (5 minutes in the case of UV irradiation and 30 minutes in case of visible irradiation, respectively). Panel B: double integration intensity of the EPR signals in function of the irradiation time.*

### 3.4 Photoluminescence (PL) characterization

The unforeseeable visible light photoactivity of synthetized ZnO leads us to perform a preliminary PL screening of the sample emission properties in order to confirm the existence of a higher number of recombination pathways in the prepared material with respect to the commercial one (Kadox). As the above described results concerning in situ-irradiation have shown that, in spite of a band gap of almost 3.3 eV (375 nm), phenomena of charge carriers separation occur in precipitated ZnO upon visible light illumination in various conditions, we performed PL measurements at various excitation wavelengths in order to obtain additional information in principle complementary to those from EPR. In Fig. 9 panel A, the PL emission spectra, performed with an excitation wavelength at 270 nm, for ZnO- and Kadox are compared.

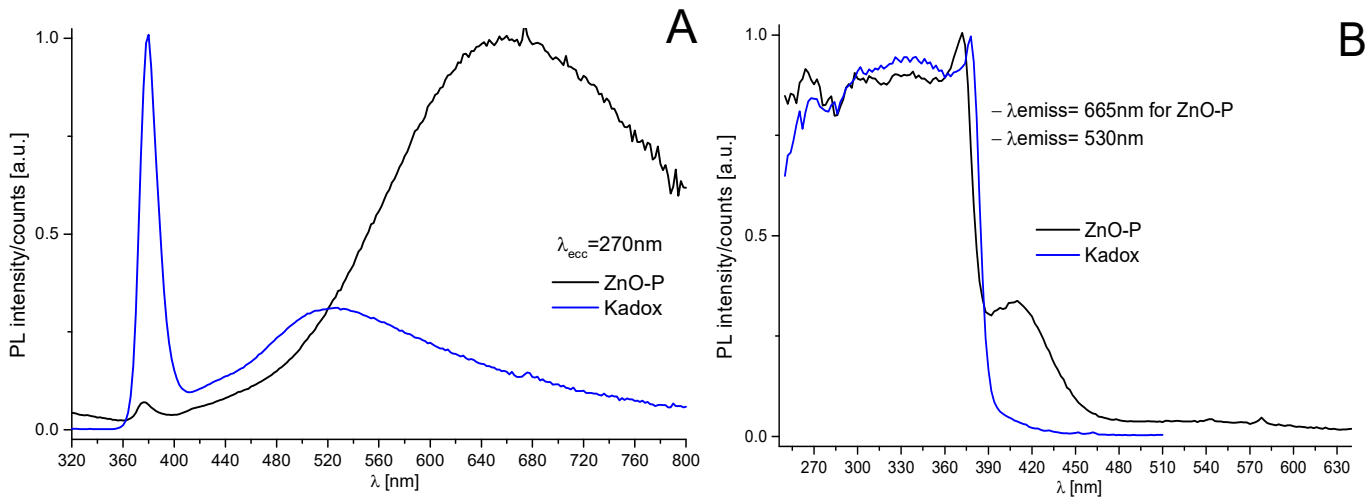


**Figure 9.** *Panel A: normalized PL emission spectra recorded with excitation wavelength fixed at 270 nm for ZnO (black line),) and Kadox (blue line). Panel B: normalized PL excitation spectra recorded at fixed emission maximum (665 nm for ZnO and 530 nm for Kadox)*

The two samples show a dramatically different emission spectrum. ZnO exhibits a broad emission band in the visible with a maximum at 665 nm (orange-red, 1.86eV) and a much weaker near band edge (NBE) recombination peak at about 375 nm (direct recombination of electrons in CB with holes in VB) [57-59]. At variance, Kadox photoluminescence is dominated by the intense NBE peak at 375 nm that is accompanied by the well-known green photoluminescence [34] with maximum at about 530 nm (2.34 eV)

The excitation spectra taken for each sample at the maximum of the emission in the visible region are reported in Fig.9, panel B. Also in this case a net difference between the two materials shows up clearly. While in the case of Kadox-ZnO the green emission peak with maximum at 530 nm can only be produced by photons with energy higher or equal to the material band gap, the orange-red photoluminescence of ZnO (665 nm) can also be generated by photons with energy lower than the band gap, roughly in the range 390-470 nm. The PL results in Fig. 9 are in accordance with what evidenced by EPR pointing to the presence of a rich defective structure in the precipitated ZnO corresponding to a variety of energy states in the band gap. The band gap population is thus much more complex in this case than in the case of the highly crystalline Kadox material.

Since the excitation spectrum in Fig. 9B has revealed that the broad orange-red emission (665 nm) typical of precipitated ZnO can be originated also by visible photons we have monitored (Fig. 10) the emission of this material using various excitation wavelengths comparing the results with that related to the excitation with light at 270 nm already shown in Fig. 9A.

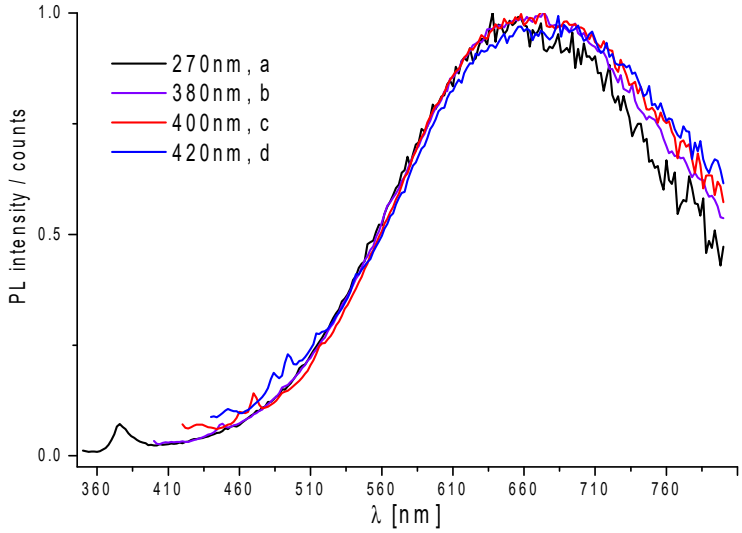


**Figure 10.** *Normalized* ZnO-P *PL emission spectra with excitation fixed at 270nm (a, black line), 380nm (b, violet line), 400nm (c, red line), 420nm (d, blue line).*

From Fig. 10 it clearly appears that all kind of excitation between λ=270nm and λ=420 nm (in two cases – 400 nm and 420 nm- with photons having energy definitely lower than the ZnO band gap value) give rise to the same orange-red emission band with maximum at 665 nm. This outcome confirms that while visible light is efficient in activating the photochemistry of the wet-synthetized ZnO; the same does not apply to Kadox-ZnO.

To summarize, in this Section we have evidenced the dominant role of the orange-red emission occurring in precipitated ZnO upon excitation by UV photons (270-380 nm) or by photons in the boundary region between UV and visible (400 nm-420 nm). This behavior is markedly different from that of Kadox in which the direct CB-VB recombination and the higher energy green emission are dominant upon excitation by UV light at 270nm and no emission can be caused by excitation frequencies in the visible range. The body of results (EPR and PL) here reported thus indicate that wet chemistry prepared ZnO has an original electronic structure responsible of a series of visible-light photoinduced transitions. Additionally, same of these transitions are effective in promoting the formation of reactive carriers (mainly holes) capable of charge transfer at the interface (Fig. 6 and 7). As it will be discussed in the next Section the reason of such a behavior must be searched in the nature and concentration of defects present in the solid.

## 4. Discussion

### 4.1 EPR of point defects in ZnO and effect of irradiation.

Although the investigation of point defects (and of paramagnetic ones in particular) in ZnO started more than fifty years ago, controversial assignments are still present in the literature. Furthermore,

an analysis of the existing literature must take into account that a number of experimental investigation is performed on materials submitted to high energy irradiations (electrons or neutrons) in order to investigate the effects of ionizing radiation on solids. The picture emerging from such investigations in terms of nature and abundance of defects in the bulk of ZnO, however, must not be confused with that of interest in the present work that considers the effects of the relatively low energy irradiation (UV, Vis) employed in photocatalysis. A thorough analysis of the defectivity in ZnO is beyond the scopes of this paper for which it is sufficient to discuss the role of the main paramagnetic defects present in the solid in the absorption of UV and, in particular, visible frequencies. For a more detailed discussion on this topic the reader is referred to the thorough review paper by Janotti and Van der Walle [60] and related works [61-64].

The EPR spectrum of ZnO obtained by precipitation, recorded after normal exposure of the material to ambient light, shows two weak signals at the opposite sides of the free electron value (Fig. 3a). The former, a symmetric line at about g= 1.96, has been the object of various assignments in the past (including the one associating this signal to oxygen vacancies). The most convincing recent interpretation is that this signal is due to electrons present in CB (or in a donor band just below the latter) deriving from the ionization of unintentional dopants of the solid such as hydrogen [50, 65] or from ionization of interstitial $Zn_i$ defects acting as shallow donors [63]. By the way this interpretation (whatever the origin of these delocalized electrons) fits with the results of this and other investigations that reports the growth of the g= 1.96 signal upon electron excitation from the VB.

At the other side of the spectrum there are weak signals in the region (2.00-2.02) assigned to zinc vacancies. Such kind of vacancies are expected to be present in a n-type semiconductor (having a relatively low formation energy) and their electronic structure is based on three nearly degenerates levels not far from the VB edge containing four electrons (the neutral $V_{Zn}$ defect) which act as deep acceptor levels being able to accept two additional electrons giving rise to $V_{Zn}^{-}$ (S=1/2 paramagnetic) and $V_{Zn}^{2-}$ (diamagnetic) respectively. These two latter defects are found at progressively higher energies into the band gap. A third feature in the background signal is a symmetric line at about g = 2.014 that has been attributed in the literature to $Pb^{3+}$ impurities [66, 67] but that, most likely, is a particular defect of the complex family of zinc vacancies [49, 68-72]. To explain this complexity it is useful to remind, just as an example, that, as shown by careful single crystal studies [70], in the wurtzitic structure of ZnO a given zinc vacancy can host two distinct types of holes respectively on axial and non-axial oxygen with distinct g values and that another defect based on an oxygen

stabilized hole shared by two Zn vacancies has also been hypothesized [47]. This explains the complexity of the hole signal observed in various experiments (Fig. 3, 5 and 7).

Whatever the exact nature of any point defect in ZnO the experiments reported in the previous section suggest few basic point characterizing the behavior of ZnO prepared by precipitation that are listed in the following:

a) this system is richer in defects in comparison with the highly crystalline Kadox-ZnO as indicated by the optical absorption that reveals a tail of the VB→CB principal transition in the first region of visible absorption.

b) the effects typical of UV-induced charge separation described by Eq.2, and reported in Fig. 3b occurs also if the irradiation is limited to the range of visible wavelengths. In particular, an abundant stabilization of electrons and holes is observed (Fig. 4 b-e) if light in the range 400-495 nm is used. The effects of this irradiation involves the stabilisation of excited electrons that is observed in terms of the increase of the EPR signal at high field (g= 1.96). The described features firmly suggest that electrons are excited mainly from the VB to populate the shallow donor band at the border with the conduction band. The existence of this region below the lower limit of the CB explains why light at 400 – 420 nm (3.10-2.95 eV) produces an effect similar to UV light in a solid having band gap $E_g$=3.28. In parallel, the increase of the signal at higher g ($g_\perp$ = 2.021, $g_{//}$ = 2.003 typical values for holes stabilized in oxides [28, 39, 40, 73-75]) witness the stabilisation of photogenerated holes, Eq. 4. The g values of this signal are very close to those accurately measured in a single crystal study and assigned to the S=1/2 $V_{Zn}^-$ centre, a hole stabilized nearby a Zn vacancy. This is manifestly due to the following process involving the photogenerated holes in the band gap

$$h^+_{(VB)} + V_{Zn}^{2-} \rightarrow V_{Zn}^- \qquad (5)$$

c) The previous equation thus indicates that more than one state at different energy are present over the limit of the VB. Accurate computational work firmly indicates that the defect highest in energy is the neutral diamagnetic $V_{Zn}^{2-}$ [60, 63] while the observed paramagnetic (S=1/2) $V_{Zn}^-$ defect is expected at lower energy. Even closer to the VB edge it should be found the neutral $V_{Zn}$ that in principle should be either a triplet state [47-49] with S=1 (not observed in the present work) or a S=0 diamagnetic state. The negative and neutral Zn vacancies are most likely involved in the recombination observed via photoluminescence that in fact show two components (Fig. 8) when the excitation light is at wavelength shorter than 420nm. The behaviour of ZnO under irradiation by UV or low wavelength visible light (400-420 nm) is resumed in Fig. 11.

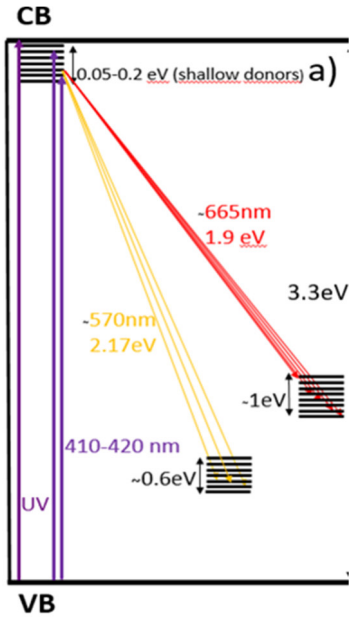


***Figure 11.*** *Schematic representation of the excitation-emission mechanism derived from PL experiments with excitation by UV or low wavelength (400-420 nm) visible light.*

In view of the presented outcomes, the most plausible explanation for the effect of irradiations with λ ≥ 455 nm and λ ≥ 495 nm (Fig. 3 and 5) seems to be the possibility to have a two-step photon absorption, already proposed in the literature for ZnO [24, 76, 77] in the past, that requires the presence of suitable intra band gap states. These intermediate states can actually be those described before, related to the presence of Zn vacancies. A $V_{Zn}^{-}$ could, in principle, host an electron promoted from the VB by a low energy photon (becoming a doubly negative $V_{Zn}^{2-}$ centre) and, in turn, the same electron could be excited to the donor band by another photon in the visible range. A similar scheme involving a bridging energy state has also been used to explain the photoactivity in the visible of doped semiconducting systems such as N-$TiO_2$ and Ce-$ZrO_2$ [8, 10, 29, 46]. To observe the double transition here discussed the polychromatic light with a wide range of frequencies (as done in the experiments reported in Fig. 3) is more efficient than the use of a single frequency in the same range. This consideration explains why using LED illumination in the red (Fig. 5) this effect of double transition is not observed.

There is however a second possibility to be considered, beside the one just described, and it is that of a contribution of an intra-band gap state different from those contemplated up to now (singly negative and doubly negative zinc vacancies). In this case the candidate for a role in the double excitation process is the defect corresponding to the symmetric signal at g = 2.014. This signal shows erratic intensity in the various samples and has not yet been discussed in this paper. The origin of

this defect can be better understood considering the results of an *ad-hoc* experiment we performed that is illustrated in Fig. 12. A sample of precipitated ZnO was prepared avoiding any contact with ambient light (ZnO-Dark). The background EPR spectrum of such material (black trace in Fig. 12) is nearly a flat line, at variance with those of the same materials submitted to a normal manipulation in ambient light which are always more intense.

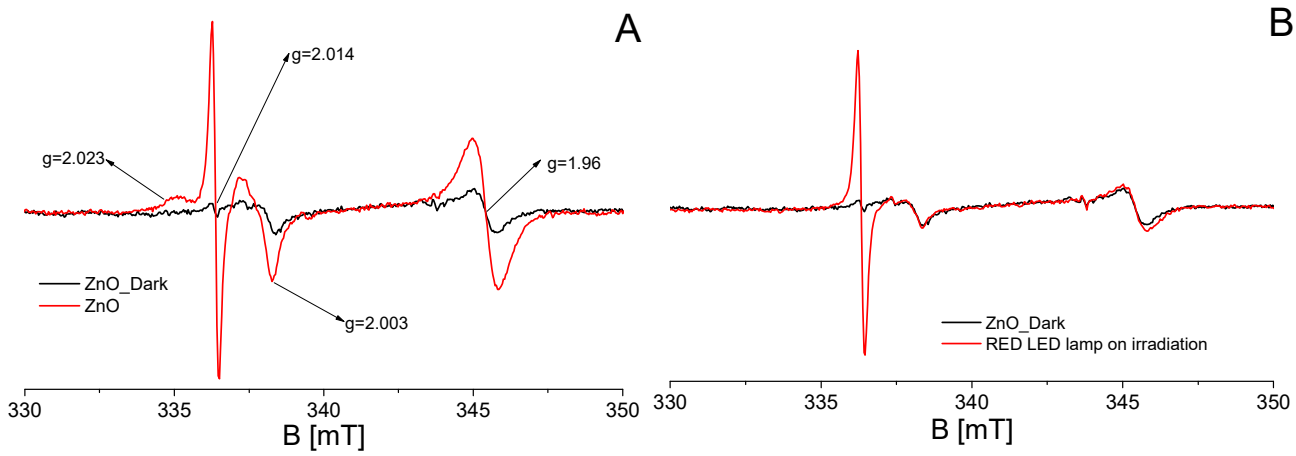


**Figure 12.** *Panel A: EPR spectra at 77K of activated ZnO_Dark before (black line) and after (red line) exposure to ambient light. Panel B: EPR spectra at 77K of activated ZnO_Dark before (black line) and after (red line) exposure to red light irradiation (LED, 5min).*

Fig. 12 compares the effects observed upon exposing the ZnO_dark sample to the normal ambient light (Panel A) or the monochromatic red light (LED, 634 nm). The difference between the two spectra is clear cut since in the former case all the signals corresponding to the previously described defects (centers having g> 2.00 (hole centers), g= 2.014 and g= 1.96) shows up while in the second case the only symmetric signal at g=2.014 appears. This signal is thus selectively generated by photons around 1.95 eV (634 nm) that are not able, as discussed before, to move electrons from the valence band to the conduction band. Its intensity is unaffected by UV-irradiation (Fig. 3b) but it drops under particular irradiations in the visible (see Fig. 4) showing its sensitivity to visible light. Both the above results point to the nature of intra-bandgap state for the defect having g=2.014.

Whatever the true nature of this defect its presence in a region mid-way between VB and CB (together with that of the other $V_{Zn}$ centers described before) contributes to explain the complex behavior of precipitated ZnO and its amazing sensitivity to visible light. Visible light irradiations are capable not only to entail a complex photochemistry reached to transitions involving intra-band gap

states, but also to generate surface active carriers (holes in particular, Fig 7) and $OH^{\bullet}$ radicals in solution (Fig. 8).

Although our description of the complex features of defective ZnO prepared by wet chemistry methods is quite schematic and partially qualitative the fact remains however that, when ZnO enters in the composition of a more complex visible light active photocatalyst like in the case of the recently reported Ce-ZnO, its peculiar interaction with visible light hereby described, must be seriously considered for the influence that the main component (ZnO) can have on the activity of the whole photocatalyst.

## 5. Conclusion

Polycrystalline zinc oxide prepared by precipitation and used (coupled with other compounds) in real photocatalyst displays a rich photochemistry in comparison with highly crystalline material prepared by direct ignition of the metal (ZnO-Kadox). This behavior is due to the presence of a rich set of intra-band gap states mainly associated to cation vacancies that origin photoluminescence properties (i.e. recombination pathway after excitation) dramatically different in the two cases.

The particular structure of the band-gap is the reason of a second peculiar property in that visible light, with photons energy lower than the band-gap value (both polychromatic - Fig. 3 and monochromatic – Fig. 5) is able to cause electron-hole separation and stabilization similar to that observed under UV illumination (Fig. 3a). This is due to a complex mechanism (not fully achieved) that excites electrons from the valence band to the conduction band by a mechanism of double or multiple excitations. The present results not only provide a useful information for a recently investigated photocatalyst based on $CeO_2$-ZnO heterojunction [19], but have an intrinsic interest shading more light on the photochemical property of zinc oxide. This material, prepared in a highly defective form, can be seen as a visible light active (VLA) system. Moreover, as shown by experiments under reactive atmosphere in aqueous suspension, a fraction of photo-formed electrons (Fig. 6) and the totality of photo-induced holes (Fig. 7) localize near the surface of the nanocrystals where they are able to react with specific scavengers or to produce free OH radicals.

## Acknowledgment

Financial support from the Italian MIUR through the PRIN Project 2015K7FZLH, SMARTNESS “Solar driven chemistry: new materials for photo- and electro-catalysis” is gratefully acknowledged, moreover, thanks to the contribution of Compagnia di San Paolo supplied under the Multi-Year Convention (2016-2018) between the University of Turin and Compagnia di San Paolo. Furthermore, we would like to thank prof.

Diwald for the fruitful discussion and for the possibility he gave us to perform PL measurements in the laboratory of the Department of Chemistry and Physics of Materials, University of Salzburg.

## References

[1] K. Hashimoto, H. Irie, A. Fujishima, $TiO_2$ Photocatalysis: a Historical Overview and Future Prospects, Jpn. J. Appl. Phys., 44 (2005) 8269-8285.
[2] D.F. Ollis, E. Pelizzetti, N. Serpone, Destruction of Water Cntaminants, Environ. Sci. Technol., 25 (1991) 1522-1529.
[3] M.R. Hoffman, S.T. Martin, W. Choi, D.W. Bahnemann, Environmental Applications of Semiconductor Photocatalysis, Chem. Rev., 95 (1995) 69-96.
[4] K. Maeda, K. Domen, Photocatalytic Water Splitting: Recent Progress and Future Challenges, J. Phys. Chem. Lett., 1 (2010) 2655-2661.
[5] X. Wang, K. Maeda, A. Thomas, K. Takanabe, G. Xin, J.M. Carlsson, K. Domen, M. Antonietti, A Metal-Free Polymeric Photocatalyst for Hydrogen Production from Water under Visible Light, Nat Mater, 8 (2009) 76-80.
[6] J. Yu, S. Wang, J. Low, W. Xiao, Enhanced Photocatalytic Performance of Direct Z-Scheme g-$C_3N_4$-$TiO_2$ Photocatalysts for the Decomposition of Formaldehyde in Air, Phys Chem Chem Phys, 15 (2013) 16883-16890.
[7] J. Zhai, T. Wang, C. Wang, D. Liu, UV-Light-Assisted Ethanol Sensing Characteristics of g-$C_3N_4$/ZnO Composites at Room Temperature, Appl. Surf. Sci., 441 (2018) 317-3323.
[8] S. Livraghi, M.C. Paganini, E. Giamello, A. Selloni, C.D. Valentin, G. Pacchioni, Origin of Photoactivity of Nitrogen-Doped Titanium Dioxide under Visible Light, J. Am. Chem. Soc., 128 (2006) 15666-15671.
[9] M. D'Arienzo, N. Siedl, A. Sternig, R. Scotti, F. Morazzoni, J. Bernardi, O. Diwald, Solar Light and Dopant-Induced Recombination Effects: Photoactive Nitrogen in TiO2 as a Case Study, J. Phys. Chem. C, 114 (2010) 18067-18072.
[10] G. Barolo, S. Livraghi, M. Chiesa, M.C. Paganini, E. Giamello, Mechanism of the Photoactivity under Visible Light of N-Doped Titanium Dioxide. Charge Carriers Migration in Irradiated N-TiO2 Investigated by Electron Paramagnetic Resonance, J. Phys. Chem. C, 116 (2012) 20887-20894.
[11] Q. Xu, L. Zhang, J. Yu, S. Wageh, A.A. Al-Ghamdi, M. Jaroniec, Direct Z-Scheme Photocatalysts: Principles, Synthesis, and Applications, Mater. Today, 21 (2018) 1042-1063.
[12] D. Huang, S. Chen, G. Zeng, X. Gong, C. Zhou, M. Cheng, W. Xue, X. Yan, J. Li, Artificial Z-Scheme Photocatalytic System: What Have Been Done and Where to Go?, Coord. Chem. Rev., 385 (2019) 44-80.
[13] P. Calza, C. Gionco, M. Giletta, M. Kalaboka, V.A. Sakkas, T. Albanis, M.C. Paganini, Assessment of the Abatement of Acelsulfame K Using Cerium Doped ZnO as Photocatalyst, J. Hazard. Mater., 323 (2016) 471-477.
[14] O. Bechambi, L. Jlaiel, W. Najjar, S. Sayadi, Photocatalytic Degradation of Bisphenol A in the Presence of Ce-ZnO: Evolution of Kinetics, Toxicity and Photodegradation Mechanism, Mater. Chem. Phys., 173 (2016) 95-105.
[15] Jin-Chung Sina, Sze-Mun Lamb, Keat-Teong Leec, A.R. Mohamed, Preparation of Cerium-Doped ZnO Hierarchical Micro/Nanospheres with Enhanced Photocatalytic Performance for Phenol Degradation under Visible Light, J. Mol. Catal. A: Chem., 409 (2015) 1-10.
[16] N.C. Birben, M.C. Paganini, P. Calza, M. Bekbolet, Photocatalytic degradation of humic acid using a novel photocatalyst: Ce-doped ZnO, Photochem. Photobiol. Sci., (2016).
[17] M.C. Paganini, D. Dalmasso, C. Gionco, V. Polliotto, L. Mantilleri, P. Calza, Beyond $TiO_2$: Cerium-Doped Zinc Oxide as a New Photocatalyst for the Photodegradation of Persistent Pollutants, ChemistrySelect, 1 (2016) 3377-3383.
[18] E. Cerrato, C. Gionco, M.C. Paganini, E. Giamello, Photoactivity Properties of ZnO Doped with Cerium Ions: an EPR Study, J. Phys. Condens. Matter., 29 (2017) 1-7.
[19] E. Cerrato, C. Gionco, M.C. Paganini, E. Giamello, E. Albanese, G. Pacchioni, Origin of Visible Light Photoactivity of the CeO2/ZnO Heterojunction, ACS Appl. Energy Mat., 1 (2018) 4247-4260.

[20] G.W. Tomlins, J.L. , Routbort, T.O. Mason, Oxygen Diffusion in Single-Crystal Zinc Oxide, J. Am. Ceram. Soc., 81 (1998) 869-876.
[21] G.W. Tomlins, J.L. Routbort, T.O. Mason, Zinc Self-Diffusion, Electrical Properties, and Defect Structure of Undoped, Single Crystal Zinc Oxide, J. Appl. Phys., 87 (2000) 117-123.
[22] H.T. Ng, B. Chen, J. Li, J. Han, M. Meyyappan, J. Wu, S.X. Li, E.E. Haller, Optical Properties of Single-Crystalline ZnO Nanowires on m-Sapphire, Appl. Phys. Lett., 82 (2003) 2023-2025.
[23] J. Li, H. Fan, X. Chen, Z. Cao, Structural and Photoluminescence of Mn-doped ZnO Single-Crystalline Nanorods Grown via Solvothermal Method, Colloids Surf., A, 349 (2009) 202-206.
[24] Y.C. Zhong, HK.S. Wong, A.B. Djurisic, Y.F. Hsu, Study of Optical Transitions in an Individual ZnO Tetrapod Using Two-Photon Photoluminescence Excitation Spectrum, Appl. Phys. B, 97 (2009) 125-128.
[25] J. Cizek, J. Valenta, P. Hruska, O. Melikhova, I. Prochazka, M. Novotny, J. Bulir, Origin of Green Luminescence in Hydrothermally Grown ZnO Single Crystals, Appl. Phys. Lett., 106 (2015) 2519021-2519024.
[26] C.W. Litton, D. C. Reynolds, T.C. Collins, Zinc Oxide Materials for Electronic and Optoelectronic Device Applications, 2011.
[27] M. Chiesa, M.C. Paganini, S. Livraghi, E. Giamello, Charge Trapping in $TiO_2$ Polymorphs as Seen by Electron Paramagnetic Resonance Spectroscopy, Phys Chem Chem Phys, 15 (2013) 9435-9447.
[28] C.D. Valentin, D. Ricci, G. Pacchioni, M. Chiesa, M.C. Paganini, E. Giamello, $O^-$ Radical Anions on Polycrystalline MgO, Surf. Sci., 521 (2002) 104-116.
[29] C. Gionco, M.C. Paganini, E. Giamello, R. Burgess, C. Di Valentin, G. Pacchioni, Cerium-Doped Zirconium Dioxide, a Visible-Light-Sensitive Photoactive Material of Third Generation, J. Phys. Chem. Lett., 5 (2014) 447-451.
[30] C. Gionco, M.C. Paganini, S. Agnoli, A.E. Reederb, E. Giamello, Structural and Spectroscopic Characterization of $CeO_2$-$TiO_2$ Mixed Oxides, J. Mater. Chem. A, 10918-10926 (2013).
[31] V. Polliotto, S. Livraghi, E. Giamello, Electron Magnetic Resonance as a Tool to Monitor Charge Separation and Reactivity in Photocatalytic Materials, Res. Chem. Intermed., 44 (2018) 3905-3921.
[32] X. Wang, L. Huang, Y. Zhao, Y. Zhang, G. Zhou, Synthesis of Mesoporous ZnO Nanosheets via Facile Solvothermal Method as the Anode Materials for Lithium-ion Batteries, Nanoscale Res. Lett., 11 (2016) 37.
[33] U. Özgür, Y.I. Alivov, C. Liu, A. Teke, M.A. Reshchikov, S. Doğan, V. Avrutin, S.J. Cho, H. Morkoç, A comprehensive review of ZnO materials and devices, J. Appl. Phys., 98 (2005) 041301.
[34] C. Drouilly, J.M. Krafft, F. Averseng, S. Casale, D. Bazer-Bachi, C. Chizallet, V. Lecocq, H. Vezin, H. Lauron-Pernot, G. Costentin, ZnO Oxygen Vacancies Formation and Filling Followed by in Situ Photoluminescence and in Situ EPR, J. Phys. Chem. C, 116 (2012) 21297-21307.
[35] L. Klucker, H. Nelkowski, Y.S. Park, M. Skibowski, T.S. Wagner, Optical Anisotropy of znO in the Ultraviolet Region, Phys Stat. Sol B, 45 (1971).
[36] J. Tauc, The Optical properties of Solids, Academic Press, NewYork, 1966.
[37] A. Mang, K. Reimann, S. Rubenacke, Band Gaps, Crystald-Field Splitting, Spin-Orbit Coupling, and Exciton Binding Energies in ZnO under Hydrostatic Pressure, Solid State Commun., 94 (1995) 251-2574.
[38] G. Pinarello, C. Pisani, A. D'Ercole, M. Chiesa, M.C. Paganini, E. Giamello, O. Diwald, $O^-$ Radical Ions on MgO as a Tool to Unravel Structure and Location of Ionic Vacancies at the Surface of Oxides: a Coupled Experimental and Theoretical Investigation, Surf. Sci. Rep., 494 (2001) 95-110.
[39] J.H. Lunsford, J.P. Jayne, Electron Paramagnetic Resonance of Oxygen on ZnO and UltravioletIrradiated MgO J. Chem. Phys., 44 (1966) 1487-1492.
[40] M. Chiesa, M.C. Paganini, E. Giamello, D.M. Murphy, O- Radical Ions on MgO: a Tool for a Structural Description of the Surface, Res. Chem. Intermed., 28 (2002) 205-214.
[41] K.A. Muller, J. Schneider, Conduction Electron Spin Resonance in Group II-VI Semiconductors and Phosphors, Phys. Lett., 4 (1963) 288-291.
[42] N.Y. Garces, N.C. Giles, L.E. Halliburton, G. Cantwell, D.B. Eason, D.C. Reynolds, D.C. Look, Production of nitrogen acceptors in ZnO by thermal annealing, Applied Physics Letters, 80 (2002) 1334-1336.
[43] V. Polliotto, E. Albanese, S. Livraghi, P. Indyka, Z. Sojka, G. Pacchioni, E. Giamello, Fifty–Fifty Zr–Ti Solid Solution with a TiO2-Type Structure: Electronic Structure and Photochemical Properties of Zirconium Titanate ZrTiO4, J. Phys. Chem. C, 121 (2017) 5487-5497.

[44] C. Gionco, M.C. Paganini, E. Giamello, O. Sacco, V. Vaiano, D. Sannino, Rare Earth Oxides in Zirconium Dioxide: How to Turn a Wide Band Gap Metal Oxide into a Visible Light Active Photocatalyst, J. Energy Chem., 26 (2017) 270-276.
[45] V. Polliotto, E. Albanese, S. Livraghi, S. Agnoli, G. Pacchioni, E. Giamello, Structural, Electronic and Photochemical Properties of Cerium-Doped Zirconium Titanate, Catal. Today, (2018).
[46] C. Gionco, M.C. Paganini, M. Chiesa, S. Maurelli, S. Livraghi, E. Giamello, Cerium Doped Zirconium Dioxide as a Potential New Photocatalytic Material. The Role of the Preparation Method on the Properties of the Material, Appl. Catal. A, 504 (2015) 338-343.
[47] A. Poppl, G. Volkel, ESR and Photo-ESR Investigations of Zinc Vacancies and Interstitial Oxygen Ions in Undoped ZnO Ceramics, phys stat. sol (a), 125 (1991) 571-581.
[48] A. Poppl, G. Volkel, ESR and Photo-ESR Investigations of the Vl Centre in ZnO Raw Material and Li-Doped ZnO Ceramic Powder, physical state solid a, 121 (1990) 1995-1204.
[49] G. Volkel, A. Poppl, B. Voigtsberg, Investigation of the Oxygen Vacancy Balance in ZnO Ceramics by Means of EPR, phys. stat. sol. (a), (1988) 295.
[50] J.M. Smith, W.E. Vehse, ESR of electron irradiated ZnO confirmation of the $F^+$center, Phys. Lett., 31A (1970) 147-148.
[51] R.B. Lal, G.M. Arnett, Electron Paramagnetic Resonance of Photosensitive Donors in ZnO, J. Phys. Soc. Jpn., 21 (1966) 2734-2735.
[52] L.S. Vlasenko, G.D. Watkins, Optical Detection of Electron Paramagnetic Resonance in Room-Temperature Electron-Irradiated ZnO, Phys. Rev. B, 71 (2005).
[53] M. Iwamoto, Y. Yoda, N. Yamazoe, T. Seiyama, Study of Metal Oxide Catalysts by Temperature Programmed Desorption. Oxygen Adsorption on Various Metal Oxides, J. Phys. Chem., 82 (1978) 2564-2570.
[54] M. Che, A.J. Tench, Characterization and Reactivity of Molecular Oxygen Species on Oxide Surfaces Adv. Catal., 32 (1983).
[55] T. Berger, O. Diwald, E. Knözinger, F. Napoli, M. Chiesa, E. Giamello, Hydrogen Activation at $TiO_2$ Anatase Nanocrystals, Chem. Phys., 339 (2007) 138-145.
[56] D. Dvoranová, V. Brezová, M. Mazúr, M.A. Malati, Investigations of metal-doped titanium dioxide photocatalysts Appl. Catal., B, 37 (2002) 91-105.
[57] B.K. Meyer, H. Alves, D.M. Hofmann, W. Kriegseis, D. Forster, F. Bertram, J. Christen, A. Hoffmann, M. Straßburg, M. Dworzak, U. Haboeck, A.V. Rodina, Bound exciton and donor–acceptor pair recombinations in ZnO, physica status solidi (b), 241 (2004) 231-260.
[58] A.B. Djurisic, A.M. Bagamadova, X. Y. Chen, ZnO Nanostructures for Optoelectronics: Material Properties and Device Applications, Prog. Quantum Electron., 34 (2010) 191-219.
[59] K. Kocsis, M. Niedermaier, T. Schwab, V. Kasparek, T. Berger, O. Diwald, Exciton Emission and Light-Induced Charge Separation in Colloidal ZnO Nanocrystals, ChemPhotoChem, 2 (2018) 994-1001.
[60] A. Janotti, C.G.V.d. Walle, Fundamentals of Zinc Oxide as a ASemiconductor, Rep. Prog. Phys., 72 (2009) 126501.
[61] A. Janotti, C.G. Van de Walle, Oxygen Vacancies in ZnO, AppL. Phys. Lett., 87 (2005) 122102.
[62] A. Janotti, C.G. Van de Walle, New insights into the role of native point defects in ZnO, J. Cryst. Growth, 287 (2006) 58-65.
[63] A. Janotti, C.G.V.d. Walle, Native Point Defects in ZnO, Phys. Rev. B, 76 (2007) 165202.
[64] C.G.V.d. Walle, Defect Analysis and Engineering in ZnO, Physica B, 308–310 (2001) 899-903.
[65] D.M. Hofmann, A. Hofstaetter, F. Leiter, H. Zhou, F. Henecker, B.K. Meyer, S.B. Orlinskii, J. Schmidt, P.G. Baranov, Hydrogen: a Relevant Shallow Donor in Zinc Oxide, Phys. Rev. Lett., 88 (2002) 0455041-0455044.
[66] G. Born, A. Hofstaetter, A. Scharmann, EPR of $Pb^{3+}$ in ZnO, Z. Physik, 240 (1970) 163-167.
[67] R. Laiho, L.S. Vlasenko, M.P. Vlasenko, Optical detection of magnetic resonance and electron paramagnetic resonance study of the oxygen vacancy and lead donors in ZnO, Journal of Applied Physics, 103 (2008) 123709.
[68] K. Senthilkumar, M. Subramanian, H. Ebisu, M. Tanemura, Y. Fujita, Trapping and Recombination Properties of the Acceptor-like VZn-H Complex Defect in ZnO, J. Phys. Chem. C, 117 (2013) 4299-4303.

[69] D. Galland, A. Herve, Temperature Dependance of the ESR Spectrum of the Zinc Vacancy in ZnO, Solid State Commun., 14 (1974) 953-956.
[70] D. Gallad, A. Herve, ESR Spectro of the Zinc Vacancy in ZnO, Phys. Lett., 33 (1970) 1-2.
[71] A.B. Djurišić, Y.H. Leung, Optical Properties of ZnO Nanostructures, Small, 2 (2006) 944-961.
[72] B. Schallenberger, A. Hausmann, Eigenst6rstellen in elektronenbestrahltem Zinkoxid, Z. Physik B, 23 (1976).
[73] M. Chiesa, E. Giamello, M.C. Paganini, Z. Sojka, D.M. Murphy, Continuous Wave Electron Paramagnetic Resonance Investigation of the Hyperfine Structure of $^{17}O_2^-$ Adsorbed on the MgO Surface, J. Chem. Phys., 116 (2002) 4266-4274.
[74] M. Chiesa, M.C. Paganini, E. Giamello, D.M. Murphy, O- radical ions onMgO: a tool for a structural description of the surface, Res. Chem. Intermed., 28 (2002) 205-214.
[75] A.M. Volodin, A.E. Cherkashin, ESR Studies of $N_2O$ Interaction with Photoinduced Centers on ZnO and MgO React. Kinet. Catal. Lett., 20 (1982) 335-338.
[76] S.L. Chen, J. Stehr, N.K. Reddy, C.W. Tu, W.M. Chen, I.A. Buyanova, Efficient Upconversion of Photoluminescence via Two-Photon Absorption in Bulk and Nanorod ZnO, Appl. Phys. B, 108 (2012) 919-924.
[77] M.K. Kavitha, K.B. Jinesh, R. Philip, P. Gopinath, H. John, Defect Engineering in ZnO Nanocones for Visible Photoconductivity and Nonlinear Absorption, Phys Chem Chem Phys, 16 (2014) 25093-25100.